EUROPEAN ORGANIZATION FOR NUCLEAR RESEARCH

L3 Note 2753
June 26, 2002

Production of Single W Bosons at LEP and Measurement of WWγ Gauge Coupling Parameters

The L3 Collaboration

Abstract

Single W boson production in electron-positron collisions is studied with the L3 detector at centre-of-mass energies between 192 GeV and 209 GeV. Events with two acoplanar hadronic jets or a single energetic lepton are selected, and the single W cross section is measured. Combining the results with measurements at lower centre-of-mass energies, the ratio of the measured cross section to the Standard Model expectation is found to be $1.09^{+0.11}_{-0.10} \pm 0.03$. From all single W data, the WWγ gauge coupling parameter κ_γ is measured to be $1.083^{+0.083}_{-0.088} \pm 0.067$.

Submitted to the 31^{st} *International Conference on High Energy Physics*
Amsterdam, Netherlands, 24-31 July 2002.

1 Introduction

At LEP, single W production [1)], $e^+e^- \to e^+\nu_e W^-$, provides one of the best experimental measurements of the trilinear gauge boson coupling parameters, in particular of the coupling parameter κ_γ [1]. In the single W process, only the electromagnetic couplings of the W boson are probed, unlike in W pair production which is also sensitive to the couplings between W and Z bosons. The single W cross section depends only on the κ_γ and λ_γ parameters [1] which are related to the magnetic dipole moment, $\mu_W = (e/(2\,m_W))\,(1+\kappa_\gamma+\lambda_\gamma)$, and the electric quadrupole moment, $Q_W = (-e/m_W^2)\,(\kappa_\gamma-\lambda_\gamma)$, of the W boson. An accurate measurement of these couplings constitutes a crucial test of the Standard Model of electroweak interactions [2,3], as demonstrated in previous studies by the LEP experiments [4–9]. Any deviation from the Standard Model predictions $\kappa_\gamma = 1$ and $\lambda_\gamma = 0$ would indicate that the W boson has an internal structure.

A particular feature of single W production is a final state positron scattered at very low polar angle, which remains undetected. Thus the detector signature of this process is two hadronic jets and a large transverse momentum imbalance, in case of hadronic W decays, or a single energetic lepton for leptonic W decays.

In this Letter the measurements of the cross sections of single W boson production at centre-of-mass energies $\sqrt{s} = 192-209$ GeV are presented. Combining the results with those obtained at lower centre-of-mass energies [5], the ratio of the measured cross section to the Standard Model expectation is determined and κ_γ and λ_γ are measured.

2 Data and Monte Carlo Samples

The data were collected with the L3 detector [10] at LEP at the mean centre-of-mass energies of 191.6, 195.5, 199.5, 201.8, 204.8, and 206.6 GeV. They correspond to an integrated luminosity of $452.6\,\mathrm{pb}^{-1}$. The separate luminosities at the six energy points are given in Table 1. In the following, the energy points are denoted as 192, 196, 200, 202, 205, and 207 GeV, respectively.

For signal studies, samples of $e^+e^- \to e^+\nu_e f\bar{f}'$ events are generated using both the GRC4F [11] and the EXCALIBUR [12] Monte Carlo generators. For background studies the following Monte Carlo programs are used: KORALW [13] ($e^+e^- \to W^+W^- \to f\bar{f}'f''\bar{f}'''$), KK2F [14] and PYTHIA [15] ($e^+e^- \to q\bar{q}(\gamma)$), KK2F [14] and KORALZ [16] ($e^+e^- \to \mu^+\mu^-(\gamma)$, $\tau^+\tau^-(\gamma)$), BHAGENE3 [17] and BHWIDE [18] for large angle Bhabha scattering ($e^+e^- \to e^+e^-(\gamma)$), TEEGG [19] for small angle Bhabha scattering ($e^+e^- \to e^+e^-\gamma$), DIAG36 [20] and PHOJET [21] for leptonic and hadronic two-photon processes, respectively, and GRC4F and EXCALIBUR for other 4-fermion final states not listed above.

The response of the L3 detector is simulated with the GEANT program [22], which takes into account the effects of energy loss, multiple scattering and showering in the detector. The GHEISHA program [23] is used to simulate hadronic interactions in the detector. Time dependent detector inefficiencies are taken into account in the simulation.

[1)] The charge conjugate reactions are understood to be included throughout the paper.

3 Signal Definition

The single W signal is defined from Monte Carlo as $e^+e^- \to e^+\nu_e f\bar{f}'$ events that satisfy the following phase-space requirements [4, 5]:

$$\begin{aligned} |\cos\theta_{e^+}| &> 0.997 \\ \min(E_f, E_{\bar{f}'}) &> 15 \text{ GeV} \\ |\cos\theta_{e^-}| &< 0.75 \quad \text{for } e^+\nu_e e^-\bar{\nu}_e \text{ events only,} \end{aligned} \tag{1}$$

where θ_{e^+} is the polar angle of the outgoing positron, and E_f and $E_{\bar{f}'}$ are the fermion energies. Generated $e^+e^- \to e^+\nu_e f\bar{f}'$ events that do not satisfy these conditions are considered as background. They come mostly from the reaction $e^+e^- \to W^+W^-$. Inside the phase-space region (1), 82% of the events have an invariant mass of the $f\bar{f}'$ pair, $m_{f\bar{f}'}$, such that $|m_{f\bar{f}'} - m_W| < 3\,\Gamma_W$, where m_W and Γ_W are the mass and the width of the W boson [24], thus indicating a high signal purity.

Signal cross sections are calculated, within the above phase-space definition, using the Monte Carlo generators GRC4F and EXCALIBUR. The latter is also used to determine selection efficiencies for the signal process and to reweight Monte Carlo events for the extraction of the gauge couplings. The main difference between the two generators is in the treatment of the masses of fermions, which are taken to be massless in EXCALIBUR. The theoretical uncertainty on the predictions for single W production cross section is estimated to be 5% [25]. This includes the effect of using a smaller electromagnetic coupling to account for the low momentum transfer of the photon in single W production and taking into account QED radiative corrections expected for a t-channel process.

4 Analysis

Events with two hadronic jets and large transverse momentum imbalance and events with single energetic electrons, muons or taus are selected. The selection criteria are optimised at different centre-of-mass energies. In the following, the analyses at the highest energies, $\sqrt{s} = 205 - 209$ GeV, are described in detail.

4.1 Hadronic Final States

Candidates for the hadronic decay of single W bosons are identified as high multiplicity hadronic events containing two acoplanar jets and no isolated leptons. The energy deposition in the electromagnetic calorimeter must be greater than 15 GeV and the total visible energy must be in the range: $0.30 < E_{vis}/\sqrt{s} < 0.65$. The transverse energy of the event is required to be greater than $0.2\,E_{vis}$. These criteria efficiently remove fermion-pair and hadronic two-photon background.

All energy clusters in an event are combined into two hadronic jets using the DURHAM jet clustering algorithm [26]. To further reject events from the radiative process $e^+e^- \to q\bar{q}(\gamma)$, the angle between the missing momentum vector and the beam axis is restricted to $|\cos\theta_{miss}| < 0.92$. In addition, the acoplanarity between the two jets must be larger than 11°.

In order to suppress background from the $e^+e^- \to W^+W^-$ process where one of the W bosons decays into leptons, events containing electrons, muons or photons with high energy are rejected.

Three jets are formed for every remaining event. The solid angle, Ω, defined by the directions of these jets is required to be less than 4.8 srad. This criterion removes part of the remaining $\tau^+\nu_\tau\,\mathrm{q}\,\bar{\mathrm{q}}'$ final states with the τ lepton decaying hadronically. Events with τ-jets are further removed by constructing a probability to identify the best candidate for a narrow τ-jet, based on cluster and track multiplicity, as well as on the mass and the momentum of the jet.

Z boson pair production in which one Z boson decays hadronically and the other into a pair of neutrinos can mimic the signal signature. A ZZ probability is constructed using the following quantities: the velocity, the invariant mass and the opening angle of the dijet system, the missing momentum, and the reconstructed neutrino energy assuming single W kinematics. A cut on this probability, shown in Figure 1, efficiently removes this background.

The numbers of events selected at each centre-of-mass energy are listed in Table 1, together with the selection efficiencies and the Standard Model expectations, calculated with EXCALIBUR.

In order to further differentiate between the signal and the $\mathrm{W^+W^-}$ background, a discriminant variable is constructed using a neural network approach [27]. The inputs to the neural network include three classes of variables. Global quantities are used, such as the velocity of the detected hadronic system, calculated as the ratio of the missing momentum and the visible energy, and the visible invariant mass. Variables based on a 2-jet topology are included, like the sum of the masses of the two jets, the ratio of the mass and the energy of the most energetic jet, the reconstructed energy of the neutrino, assuming single W kinematics, the missing momentum, the rescaled invariant mass and velocity of the hadronic system, and the angle between the two jets. Finally, variables assuming a 3-jet topology are considered: the solid angle Ω, the DURHAM parameter y_{23} for which the number of jets in the event changes from two to three, and the minimal opening angle between any two jets. Figure 2 shows the output of the neural network used in the subsequent analysis.

4.2 Leptonic Final States

Single W candidates where the W boson decays leptonically have the distinct signature of one high energy lepton and no other significant activity in the detector. Events with one charged lepton identified either as electron, muon or hadronic τ-jet [5] are selected. Events containing well measured tracks that are not associated to the lepton are rejected.

Several selection criteria are applied to suppress background from two-fermion production $\mathrm{e^+e^-} \to \ell^+\ell^-(\gamma)$. The angle between the lepton candidate and any track or calorimetric object that could be assigned to a second particle in the opposite hemisphere is required to be less than 2.8 rad for electron and muon candidates and less than 2.4 rad for hadronic tau candidates. Furthermore, the visible mass of all energy clusters must be less than $0.1\sqrt{s}$. No more than 10 GeV are allowed to be deposited in the low angle calorimeters.

In single electron final states, the electron energy must exceed 92% of the total energy, calculated as the sum of the lepton energy and the energies of all neutral clusters in the event. The polar angle is restricted to the central detector region, $|\cos\theta_\mathrm{e}| < 0.75$. These requirements reduce the contribution from Bhabha and Compton scattering and from the process $\mathrm{e^+e^-} \to \mathrm{e^+e^-}\nu\bar{\nu}$ where the $\mathrm{e^+e^-}$ pair originates from a low-mass virtual photon. Converted photons from the process $\mathrm{e^+e^-} \to \nu\bar{\nu}\gamma$ might fake a single electron. Since configurations with the $\nu\bar{\nu}$ pair originating from a Z boson are preferred, the mass recoiling against the single electron candidate is required to be incompatible with the Z boson mass and to exceed $0.48\sqrt{s}$.

For single muon final states, the muon energy, measured in the muon chambers and in the

central tracker, is required to be greater than 90% of the total energy. The fiducial volume for this analysis is defined to be $|\cos\theta_\mu| < 0.86$. Additional requirements are put on the missing transverse momentum, $p_\perp^{miss} \geq 0.08\sqrt{s}$, and on the mass recoiling against the muon, $M_{rec}/\sqrt{s} \leq 0.91$.

Single tau candidates are accepted in a polar angular range of $|\cos\theta_\tau| < 0.75$. The number of charged tracks reconstructed in the central tracking system and associated with the hadronic tau must be either 1 or 3. Background is further reduced by requiring the mass recoiling against the tau to be in the range: $0.55 \leq M_{rec}/\sqrt{s} \leq 0.93$.

The trigger efficiencies are determined directly from the data to be 90%, 95%, and 98% for the electron, muon and tau channels, respectively. The numbers of observed and expected events as well as the selection efficiencies are summarised in Table 1. Figure 3 shows the lepton energy spectra for the selected events.

5 Cross Section Measurement

The cross section of the signal process at each energy point is determined by a binned maximum likelihood fit to the distributions of the neural network output in the hadronic decay channel and of the combined lepton energy distributions in the lepton channel. The background shapes and normalisations are fixed to the Monte Carlo prediction.

The measured signal cross sections for the phase space region (1) are summarised in Table 2 for the six centre-of-mass energies. When combining the hadronic and leptonic channels, Standard Model values for the branching fractions of the W boson [28] are assumed. The measured cross section values are consistent with the Standard Model expectations calculated with GRC4F and EXCALIBUR. The dependence of the cross section on the centre-of-mass energy agrees well with the predictions, as shown in Figure 4.

The systematic uncertainties on the cross section measurements for the hadronic and leptonic channels are summarised in Table 3. A significant contribution arises from the difference between the GRC4F and EXCALIBUR signal modelling, estimated by comparing the signal efficiencies obtained with the two Monte Carlo programs.

In the hadronic channel the uncertainty due to the choice of the neural network structure is tested by changing the parameters of the network. Effects of detector resolution and calibration are studied by smearing and shifting the kinematic variables that are fed into the network. They give a negligible contribution to the systematic uncertainty. The identification of leptons is studied using control data samples of two-fermion production and differences between data and the simulation are taken into account in the systematics.

Limited Monte Carlo statistics introduce uncertainties on the signal efficiency and the expected background levels. In addition, the $\mathrm{W^+W^-}$ and ZZ background cross sections are varied within the uncertainties on the theoretical predictions of 0.5% and 2% [25], respectively. As a cross-check, a fit of the $\mathrm{W^+W^-}$ cross section is performed, keeping the single W contribution fixed to the Standard Model prediction. It agrees, within the statistical accuracy, with the expectation for $\mathrm{W^+W^-}$ production. Finally, a variation of the bin sizes of the fitted distributions is taken into account.

The results at different centre-of-mass energies are further analysed in terms of the ratio, R, of the measured cross section, $\sigma^{meas}_{\mathrm{e\nu W}}$, to the theoretical expectation, $\sigma^{theo}_{\mathrm{e\nu W}}$, calculated with GRC4F. The R value is extracted by combining the individual likelihood functions of the cross section measurements. Systematic uncertainties and correlations between them are taken into account in the combination. Uncertainties on the background cross sections are treated as

correlated between all data sets. Systematics originating from the signal modelling are taken as correlated between energy points, but uncorrelated between the hadronic and leptonic channels. All other systematic contributions are assumed to be uncorrelated.

A fit to all data at $\sqrt{s} = 161 - 209$ GeV yields

$$R \;=\; \sigma^{meas}_{\mathrm{e\nu W}}/\sigma^{theo}_{\mathrm{e\nu W}} = 1.09^{+0.11}_{-0.10} \pm 0.03\,,$$

where the first uncertainty is statistical and the second systematic. Good agreement of the cross section measurements with the Standard Model expectation is found.

6 WWγ Gauge Couplings

Figure 4 shows the sensitivity of the single W cross section to anomalous values of κ_γ. A binned maximum likelihood fit to the neural network output distributions and the lepton energy spectra is used to extract κ_γ and λ_γ. In the fit, each Monte Carlo event is assigned a weight that depends on the generated event kinematics and the values of κ_γ and λ_γ. The dependence of the W pair background on the gauge couplings is also taken into account.

Assuming custodial $SU(2) \times U(1)$ gauge symmetry, the Z boson gauge boson couplings g_1^{Z}, κ_{Z} and λ_{Z} are constrained to: $\kappa_{\mathrm{Z}} = g_1^{\mathrm{Z}} - \tan^2\theta_{\mathrm{w}} \times (\kappa_\gamma - 1)$ and $\lambda_{\mathrm{Z}} = \lambda_\gamma$. In addition, the weak charge of the W bosons is assumed to be one, $g_1^{\mathrm{Z}} = 1$. These constraints are applied in the fit, but affect only the background contributions, as the signal process depends on κ_γ and λ_γ only.

Similar systematic error sources as for the cross section determination are studied for the coupling measurement. The dominant systematic uncertainty arises from the difference in the signal efficiency estimated using the GRC4F and EXCALIBUR Monte Carlo generators. The effect on κ_γ and λ_γ is found to be 0.047 and 0.063, respectively. Both programs agree on the ratio of cross sections with and without anomalous values of the gauge couplings.

The theoretical uncertainty of 5% [25] on the total cross section for single W boson production translates into a systematic variation of 0.042 for κ_γ and 0.010 for λ_γ. The influence of the uncertainties [25] on the $\mathrm{W^+W^-}$ and ZZ cross section predictions is found to be 0.002 on κ_γ and 0.010 on λ_γ.

The systematic uncertainties due to the signal modelling and the background estimation are taken as correlated between the different data sets. Systematic effects arising from limited Monte Carlo statistics, event selection and detector description are assumed to be uncorrelated between the individual channels and centre-of-mass energies. These effects mainly affect the overall normalisation of the cross sections in the individual data sets.

Single W production is particularly sensitive to the gauge coupling κ_γ. The parameter λ_γ is therefore set to zero in the fit for κ_γ. Combining the new data with those collected at $\sqrt{s} = 161 - 189$ GeV [5], yields:

$$\kappa_\gamma \;=\; 1.083^{+0.083}_{-0.088} \pm 0.067\,.$$

This result agrees well with the Standard Model value of unity. The likelihood distributions, shown in Figure 5 a, proof that the single W data dominates the determination of κ_γ. The limits on κ_γ at 95% confidence level are:

$$0.86 \;<\; \kappa_\gamma \;<\; 1.29\,.$$

Unlike the measurement of κ_γ, the determination of λ_γ is mainly driven by a variation of the $\mathrm{W^+W^-}$ background and less by the single W signal, as illustrated in the likelihood distributions shown in Figure 5 b.

Varying both couplings κ_γ and λ_γ freely in the fit yields:

$$\begin{array}{rcl@{\qquad}rcl} \kappa_\gamma & = & 1.03^{+0.10}_{-0.10}\pm 0.06 & 0.73 & < \kappa_\gamma < & 1.31 \ (95\%\,\text{C.L.}) \\ \lambda_\gamma & = & 0.32^{+0.12}_{-0.20}\pm 0.07 & -0.46 & < \lambda_\gamma < & 0.62 \ (95\%\,\text{C.L.}) \ , \end{array}$$

with a correlation of -13%. The corresponding 68% and 95% confidence level contours are shown in Figure 6. These results represent a considerable improvement in the accuracy compared to our previous measurements [5] and are complementary to those determined at the Tevatron [31,32] and from $\mathrm{W^+W^-}$ production at LEP [7,9,29,30], in particular for the parameter κ_γ.

Appendix

The results on the single W cross-section are also expressed in a different phase space region. Single W production can alternatively be defined as the complete t-channel subset of Feynman diagrams contributing to the $\mathrm{e^+\nu_e f\,\bar{f}'}$ final states with additional kinematic cuts. For $\mathrm{e^+\nu_e q\,\bar{q}'}$ final states the invariant mass of the $\mathrm{q\,\bar{q}'}$ pair is required to be greater than 45 GeV. In case of $\mathrm{e^+\nu_e \ell^-\bar{\nu}_\ell}$ the energy of the lepton, E_{ℓ^-}, must be greater than 20 GeV. For the $\mathrm{e^+\nu_e e^-\bar{\nu}_e}$ final state additional angular cuts are applied: $|\cos\theta_{\mathrm{e^+}}| > 0.95$ and $|\cos\theta_{\mathrm{e^-}}| < 0.95$. The measured cross sections corresponding to these phase space conditions are given in Table 4.

References

[1] T. Tsukamoto and Y. Kurihara, Phys. Lett. **B 389** (1996), 162.

[2] S. L. Glashow, Nucl. Phys. **22** (1961) 579; S. Weinberg, Phys. Rev. Lett. **19** (1967) 1264; A. Salam, "Elementary Particle Theory", Ed. N.Svartholm, Stockholm, "Almquist and Wiksell", (1968), 367.

[3] M. Veltman, Nucl. Phys. **B 7** (1968) 637; G. M. 't Hooft, Nucl. Phys. **B 35** (1971) 167; G. M. 't Hooft and M. Veltman, Nucl. Phys. **B 44** (1972) 189; Nucl. Phys. **B 50** (1972) 318.

[4] L3 Collab., M. Acciarri *et al.*, Phys. Lett. **B 403** (1997) 168.

[5] L3 Collab., M. Acciarri *et al.*, Phys. Lett. **B 436** (1998) 417; M. Acciarri *et al.*, Phys. Lett. **B 487** (2000) 229.

[6] ALEPH Collab., R. Barate *et al.*, Phys. Lett. **B 462** (1999) 389.

[7] ALEPH Collab., A. Heister *et al.*, Eur. Phys. J. **C 21** (2001) 423.

[8] DELPHI Collab., P. Abreu *et al.*, Phys. Lett. **B 459** (1999) 382; P. Abreu *et al.*, Phys. Lett. **B 515** (2001) 238.

[9] DELPHI Collab., P. Abreu *et al.*, Phys. Lett. **B 502** (2001)9.

[10] L3 Collab., B. Adeva *et al.*, Nucl. Instr. and Meth. **A 289** (1990) 35; M. Chemarin *et al.*, Nucl. Instr. and Meth. **A 349** (1994) 345; M. Acciarri *et al.*, Nucl. Instr. and Meth. **A 351** (1994) 300; G. Basti *et al.*, Nucl. Instr. and Meth. **A 374** (1996) 293; I.C. Brock *et al.*, Nucl. Instr. and Meth. **A 381** (1996) 236; A. Adam *et al.*, Nucl. Instr. and Meth. **A 383** (1996) 342.

[11] J. Fujimoto *et al.*, Comp. Phys. Comm. **100** (1997) 128.

[12] F. A. Berends, R. Pittau and R. Kleiss, Comp. Phys. Comm. **85** (1995) 437.

[13] M. Skrzypek *et al.*, Comp. Phys. Comm. **94** (1996) 216; M. Skrzypek *et al.*, Phys. Lett. **B 372** (1996) 289.

[14] S. Jadach, B. F. L. Ward and Z. Wąs, Comp. Phys. Comm. **130** (2000) 260.

[15] T. Sjöstrand, preprint CERN-TH/7112/93 (1993), revised 1995; T. Sjöstrand, Comp. Phys. Comm. **82** (1994) 74.

[16] S. Jadach, B.F.L. Ward and Z. Wąs, Comp. Phys. Comm. **79** (1994) 503.

[17] J. H. Field, Phys. Lett. **B 323** (1994) 432; J. H. Field and T. Riemann, Comp. Phys. Comm. **94** (1996) 53.

[18] S. Jadach, W. Placzek und B.F.L. Ward, Phys. Lett. **B 390** (1997) 298.

[19] D. Karlen, Nucl. Phys. **B 289** (1987) 23.

[20] F. A. Berends and R. Kleiss, Nucl. Phys. **B 253** (1985) 441.

[21] R. Engel, Z.Phys. **C 66** (1995) 203; R. Engel, J. Ranft and S. Roesler, Phys. Rev. **D 52** (1995) 1459.

[22] R. Brun *et al.*, preprint CERN DD/EE/84-1 (1984), revised 1987.

[23] H. Fesefeldt, RWTH Aachen report PITHA 85/02 (1985).

[24] The Particle Data Group, D.E. Groom, *et al.*, Eur. Phys. J. **C 15** (2000) 250.

[25] M. W. Grünewald, G. Passarino, *et al.*, preprint hep-ph/0005309.

[26] S. Catani *et al.*, Phys. Lett. **B 269** (1991) 432; S. Bethke *et al.*, Nucl. Phys. **B 370** (1992) 310.

[27] L. Lönnblad, C. Peterson and T. Rögnvaldsson, Nucl. Phys. **B 349** (1991) 675; C. Peterson *et al.*, Comp. Phys. Comm. **81** (1994) 185.

[28] W. Beenakker *et al.*, in *Physics at LEP 2*, report CERN 96-01 (1996), eds G. Altarelli, T. Sjöstrand and F. Zwirner, Vol. 1, p. 79.

[29] L3 Collab., M. Acciari *et al.*, Phys. Lett. **B 467** (1999) 171.

[30] OPAL Collab., G. Abbiendi *et al.*, Eur. Phys. J. **C 19** (2001) 1.

[31] DØ Collab., B. Abbott *et al.*, Phys. Rev. **D 60** (1999) 072002.

[32] CDF Collab., F. Abe *et al.*, Phys. Rev. Lett. **75** (1995) 1017.

	$\sqrt{s} = 192$ GeV		$\mathcal{L} = 29.7\,\mathrm{pb}^{-1}$		$\sqrt{s} = 196$ GeV		$\mathcal{L} = 83.7\,\mathrm{pb}^{-1}$	
Final State	N_{data}	N_{MC}^{tot}	N_{MC}^{sign}	ε [%]	N_{data}	N_{MC}^{tot}	N_{MC}^{sign}	ε [%]
$\mathrm{e}^+\nu_\mathrm{e}\mathrm{q}\,\bar{\mathrm{q}}'$	26	26.4 ± 0.3	5.8 ± 0.1	47.4	92	79.7 ± 0.7	17.6 ± 0.2	48.6
$\mathrm{e}^+\nu_\mathrm{e}\mathrm{e}^-\bar{\nu}_\mathrm{e}$	3	2.4 ± 0.1	1.34 ± 0.02	73.2	9	7.9 ± 0.2	4.17 ± 0.06	74.0
$\mathrm{e}^+\nu_\mathrm{e}\mu^-\bar{\nu}_\mu$	1	1.8 ± 0.3	1.12 ± 0.01	53.3	4	4.3 ± 0.2	3.46 ± 0.04	53.6
$\mathrm{e}^+\nu_\mathrm{e}\tau^-\bar{\nu}_\tau$	1	0.8 ± 0.1	0.48 ± 0.01	30.5	2	2.6 ± 0.1	1.44 ± 0.03	30.3
$\mathrm{e}^+\nu_\mathrm{e}\ell^-\bar{\nu}_\ell$	5	5.0 ± 0.3	2.9 ± 0.1	51.6	15	14.8 ± 0.3	9.1 ± 0.1	51.7

	$\sqrt{s} = 200$ GeV		$\mathcal{L} = 82.8\,\mathrm{pb}^{-1}$		$\sqrt{s} = 202$ GeV		$\mathcal{L} = 37.0\,\mathrm{pb}^{-1}$	
Final State	N_{data}	N_{MC}^{tot}	N_{MC}^{sign}	ε [%]	N_{data}	N_{MC}^{tot}	N_{MC}^{sign}	ε [%]
$\mathrm{e}^+\nu_\mathrm{e}\mathrm{q}\,\bar{\mathrm{q}}'$	77	82.4 ± 0.8	19.3 ± 0.2	49.6	46	36.9 ± 0.4	9.1 ± 0.1	51.5
$\mathrm{e}^+\nu_\mathrm{e}\mathrm{e}^-\bar{\nu}_\mathrm{e}$	13	7.8 ± 0.3	4.33 ± 0.08	71.9	6	3.6 ± 0.1	2.02 ± 0.04	75.0
$\mathrm{e}^+\nu_\mathrm{e}\mu^-\bar{\nu}_\mu$	3	4.9 ± 0.2	3.59 ± 0.04	52.1	1	2.3 ± 0.1	1.70 ± 0.03	53.6
$\mathrm{e}^+\nu_\mathrm{e}\tau^-\bar{\nu}_\tau$	2	2.4 ± 0.1	1.52 ± 0.03	30.1	1	1.2 ± 0.1	0.73 ± 0.02	31.3
$\mathrm{e}^+\nu_\mathrm{e}\ell^-\bar{\nu}_\ell$	18	15.2 ± 0.3	9.4 ± 0.2	50.7	8	7.0 ± 0.2	4.5 ± 0.1	52.3

	$\sqrt{s} = 205$ GeV		$\mathcal{L} = 79.0\,\mathrm{pb}^{-1}$		$\sqrt{s} = 207$ GeV		$\mathcal{L} = 139.1\,\mathrm{pb}^{-1}$	
Final State	N_{data}	N_{MC}^{tot}	N_{MC}^{sign}	ε [%]	N_{data}	N_{MC}^{tot}	N_{MC}^{sign}	ε [%]
$\mathrm{e}^+\nu_\mathrm{e}\mathrm{q}\,\bar{\mathrm{q}}'$	79	88.4 ± 1.0	19.9 ± 0.2	51.2	163	158.0 ± 1.8	38.1 ± 0.4	52.9
$\mathrm{e}^+\nu_\mathrm{e}\mathrm{e}^-\bar{\nu}_\mathrm{e}$	7	7.1 ± 0.4	3.9 ± 0.1	70.2	12	12.9 ± 0.7	7.1 ± 0.1	72.8
$\mathrm{e}^+\nu_\mathrm{e}\mu^-\bar{\nu}_\mu$	2	3.8 ± 0.2	3.1 ± 0.1	47.8	9	7.0 ± 0.2	5.9 ± 0.1	49.8
$\mathrm{e}^+\nu_\mathrm{e}\tau^-\bar{\nu}_\tau$	4	2.2 ± 0.2	1.7 ± 0.1	25.9	4	3.7 ± 0.4	2.0 ± 0.1	24.7
$\mathrm{e}^+\nu_\mathrm{e}\ell^-\bar{\nu}_\ell$	13	13.1 ± 0.5	8.7 ± 0.1	46.7	25	23.6 ± 0.9	16.0 ± 0.2	47.8

Table 1: The number of selected candidates for single W boson production, N_{data}, compared to the total number of expected events, N_{MC}^{tot}, for each decay channel of the W boson. The expected number of signal events, N_{MC}^{sign}, and the selection efficiencies, ε, are also shown. The uncertainties quoted are due to Monte Carlo statistics.

$\sqrt{s}$ [GeV]	192	196	200	202	205	207
$\sigma_{e\nu q\bar{q}'}$	$0.66\,^{+0.35}_{-0.29} \pm 0.03$	$0.52\,^{+0.19}_{-0.18} \pm 0.03$	$0.29\,^{+0.18}_{-0.16} \pm 0.02$	$0.87\,^{+0.32}_{-0.28} \pm 0.05$	$0.35\,^{+0.20}_{-0.17} \pm 0.02$	$0.53\,^{+0.15}_{-0.14} \pm 0.03$
$\sigma^{\mathrm{GRC4F}}_{e\nu q\bar{q}'}$	0.406	0.435	0.465	0.480	0.483	0.496
$\sigma^{\mathrm{EXCALIBUR}}_{e\nu q\bar{q}'}$	0.398	0.439	0.461	0.474	0.527	0.544
$\sigma_{e\nu\ell\nu}$	$0.21\,^{+0.17}_{-0.12} \pm 0.02$	$0.22\,^{+0.10}_{-0.08} \pm 0.01$	$0.30\,^{+0.11}_{-0.09} \pm 0.01$	$0.29\,^{+0.17}_{-0.13} \pm 0.01$	$0.21\,^{+0.11}_{-0.09} \pm 0.01$	$0.27\,^{+0.08}_{-0.07} \pm 0.01$
$\sigma^{\mathrm{GRC4F}}_{e\nu\ell\nu}$	0.182	0.196	0.209	0.215	0.225	0.231
$\sigma^{\mathrm{EXCALIBUR}}_{e\nu\ell\nu}$	0.195	0.213	0.229	0.232	0.237	0.243
$\sigma_{e\nu W}$	$0.83\,^{+0.36}_{-0.31} \pm 0.04$	$0.73\,^{+0.21}_{-0.19} \pm 0.03$	$0.67\,^{+0.20}_{-0.18} \pm 0.03$	$1.12\,^{+0.34}_{-0.31} \pm 0.04$	$0.59\,^{+0.22}_{-0.19} \pm 0.03$	$0.81\,^{+0.16}_{-0.15} \pm 0.03$
$\sigma^{\mathrm{GRC4F}}_{e\nu W}$	0.588	0.631	0.674	0.695	0.721	0.727
$\sigma^{\mathrm{EXCALIBUR}}_{e\nu W}$	0.593	0.652	0.689	0.706	0.761	0.788

Table 2: Measured cross sections in pb of the single W process at centre-of-mass energies between 192 GeV and 207 GeV. The results for hadronically and leptonically decaying W bosons, as well as their combination are shown. The first uncertainty is statistical and the second systematic. Also listed are the Standard Model predictions calculated with the GRC4F and the EXCALIBUR Monte Carlo programs. The theoretical predictions presented here are calculated with a statistical accuracy of $0.2\% - 1.0\%$. The current theoretical uncertainty on the single W cross section is of the order of 5% [25] .

Source of uncertainty	Final state	
	$W^- \to q\bar{q}'$	$W^- \to \ell^-\bar{\nu}_\ell$
Signal modelling	3.2	2.1
Lepton identification	—	1.5
Neural network	3.0	—
Signal Monte Carlo statistics	1.0 – 1.2	1.6 – 2.1
Background Monte Carlo statistics	1.1 – 3.4	1.9 – 6.0
Background cross section	0.6	0.4
Variation of binning	1.0	1.5
Total systematics	4.8 – 5.4	3.9 – 6.9

Table 3: Relative systematic uncertainties in per cent on the determination of the single W cross section at $\sqrt{s} = 192 - 209$ GeV for the hadronic and leptonic final states. The uncertainties due to Monte Carlo statistics vary at the different centre-of-mass energies.

$\sqrt{s}$ [GeV]	$\sigma_{e\nu q\bar{q}'}$	$\Delta\sigma^{exp}_{stat}$	$\sigma^{\mathrm{GRC4F}}_{e\nu q\bar{q}'}$	$\sigma_{e\nu W}$	$\Delta\sigma^{exp}_{stat}$	$\sigma^{\mathrm{GRC4F}}_{e\nu W}$
183	$0.58^{+0.23}_{-0.20} \pm 0.04$	0.21	0.42	$0.80^{+0.28}_{-0.25} \pm 0.05$	0.26	0.63
189	$0.52^{+0.14}_{-0.13} \pm 0.03$	0.14	0.46	$0.69^{+0.16}_{-0.14} \pm 0.04$	0.15	0.69
192	$0.84^{+0.44}_{-0.37} \pm 0.05$	0.41	0.49	$1.07^{+0.47}_{-0.40} \pm 0.05$	0.45	0.73
196	$0.66^{+0.24}_{-0.22} \pm 0.03$	0.21	0.52	$0.93^{+0.26}_{-0.24} \pm 0.03$	0.24	0.78
200	$0.37^{+0.22}_{-0.20} \pm 0.02$	0.22	0.56	$0.86^{+0.25}_{-0.23} \pm 0.04$	0.25	0.84
202	$1.10^{+0.34}_{-0.35} \pm 0.07$	0.35	0.58	$1.44^{+0.44}_{-0.39} \pm 0.05$	0.38	0.87
205	$0.42^{+0.25}_{-0.21} \pm 0.03$	0.24	0.61	$0.76^{+0.28}_{-0.25} \pm 0.03$	0.28	0.91
207	$0.66^{+0.19}_{-0.17} \pm 0.04$	0.19	0.62	$1.04^{+0.20}_{-0.19} \pm 0.04$	0.21	0.94

Table 4: Measured hadronic and total cross sections at $\sqrt{s} = 183 - 189$ GeV [4,5] and at $\sqrt{s} = 192 - 207$ GeV using an alternative signal definition of the single W process. The first uncertainty is statistical and the second systematic. Also listed are the expected statistical uncertainties, $\Delta\sigma^{exp}_{stat}$, at each centre-of-mass energy and the Standard Model predictions calculated with GRC4F. All cross sections are given in pb.

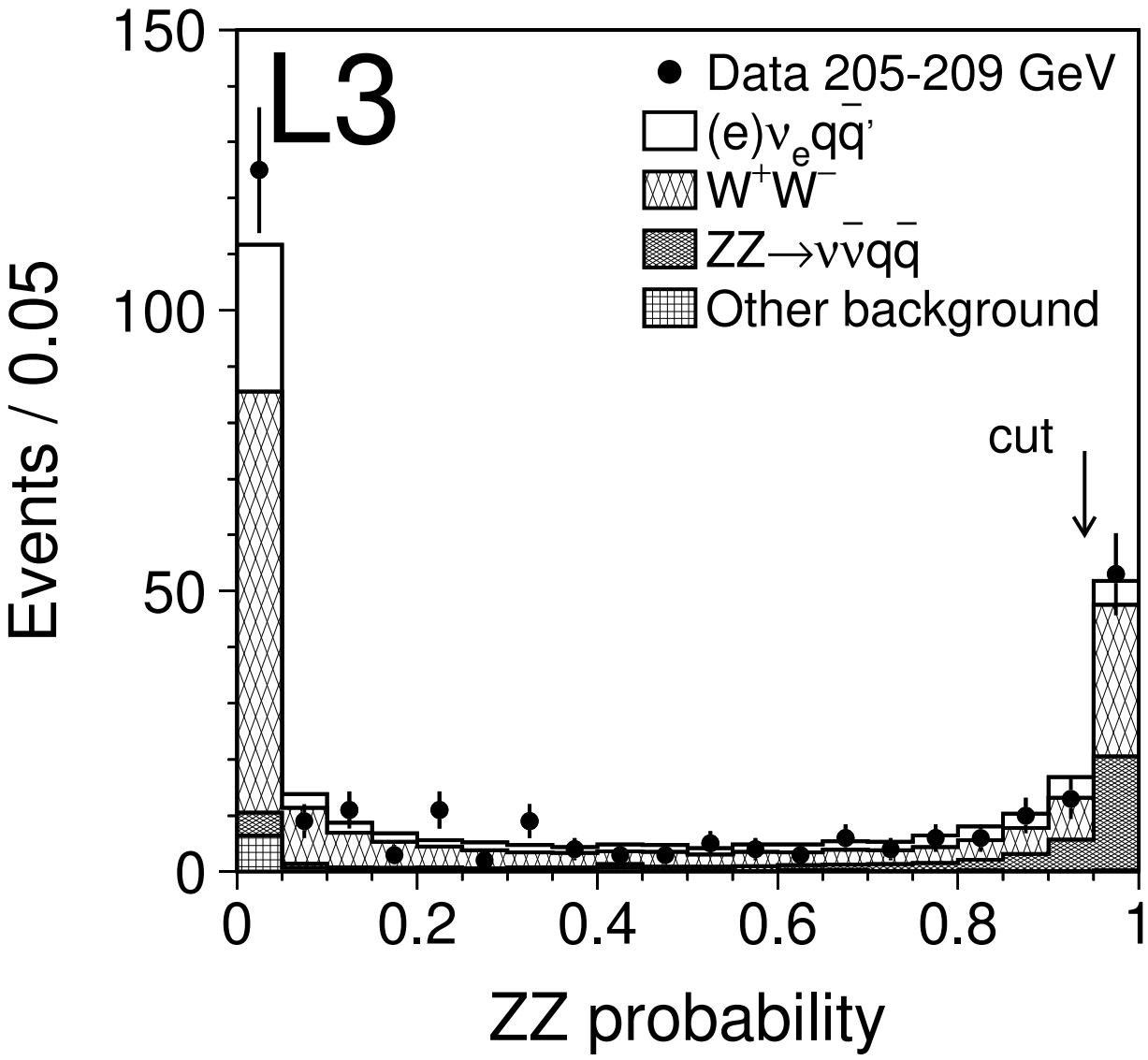

Figure 1: Distribution of the ZZ probability for the selected hadronic events at $\sqrt{s} = 205 - 209$ GeV and Monte Carlo expectations. The arrow indicates the position of the applied cut.

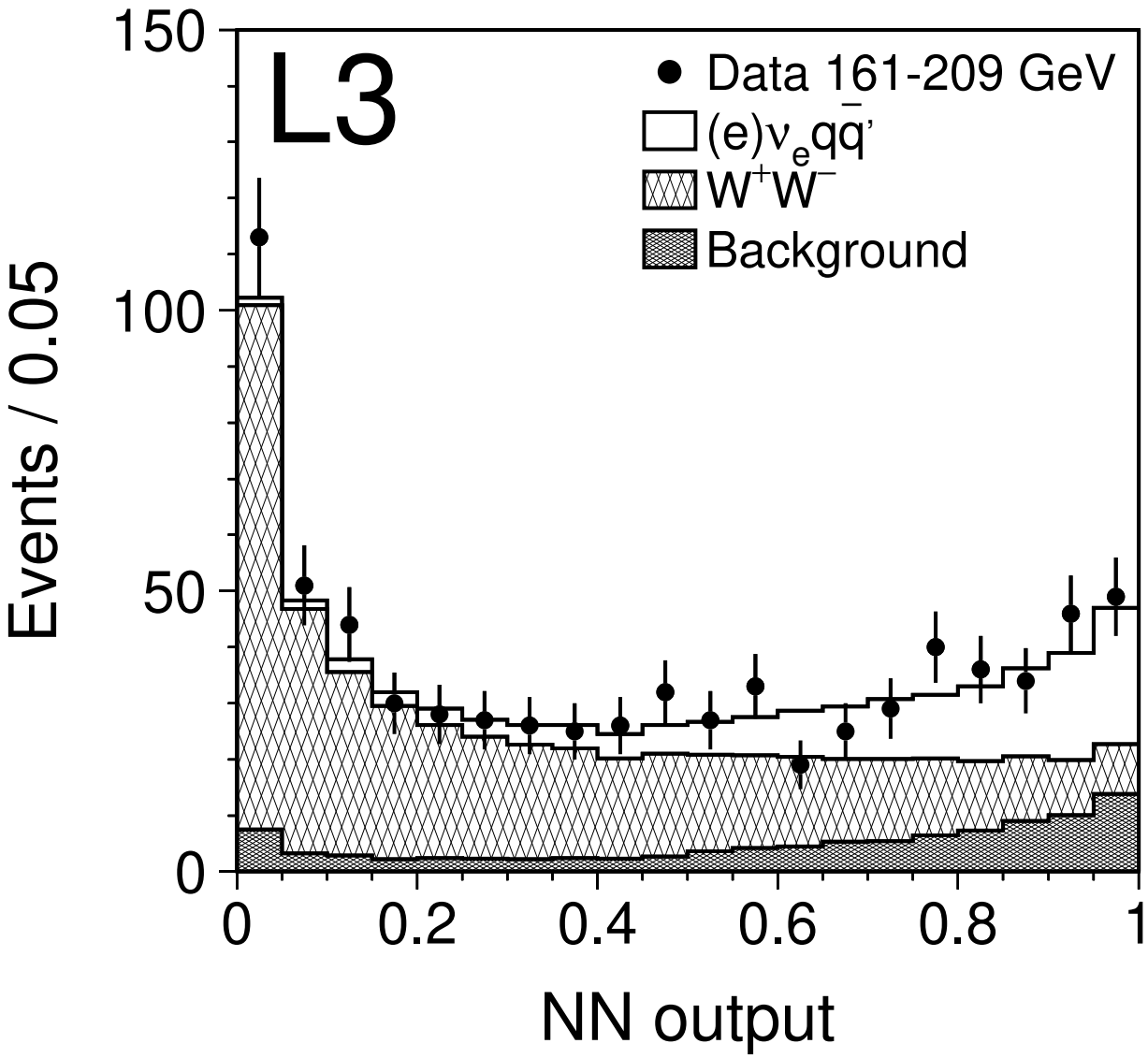

Figure 2: Distribution of the output of the neural network, used to identify hadronic single W decays. The data collected at $\sqrt{s} = 161 - 209$ GeV are shown, together with the background contributions and the expected signal.

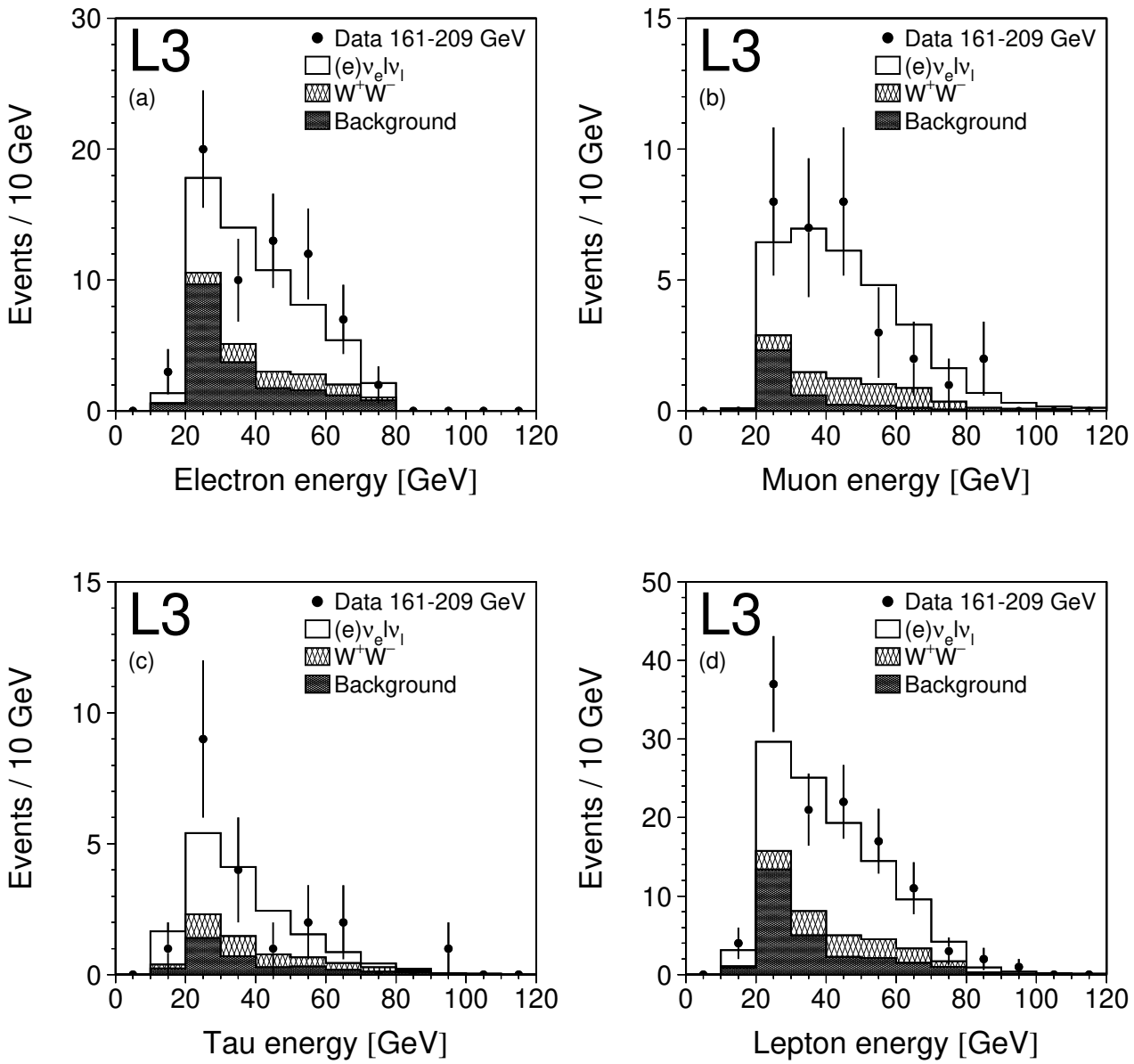

Figure 3: The energy spectrum of the lepton candidates, selected as (a) electrons, (b) muons or (c) hadronic τ-jets, and their sum (d). Data measured at $\sqrt{s} = 161 - 209$ GeV are presented, together with Monte Carlo expectations.

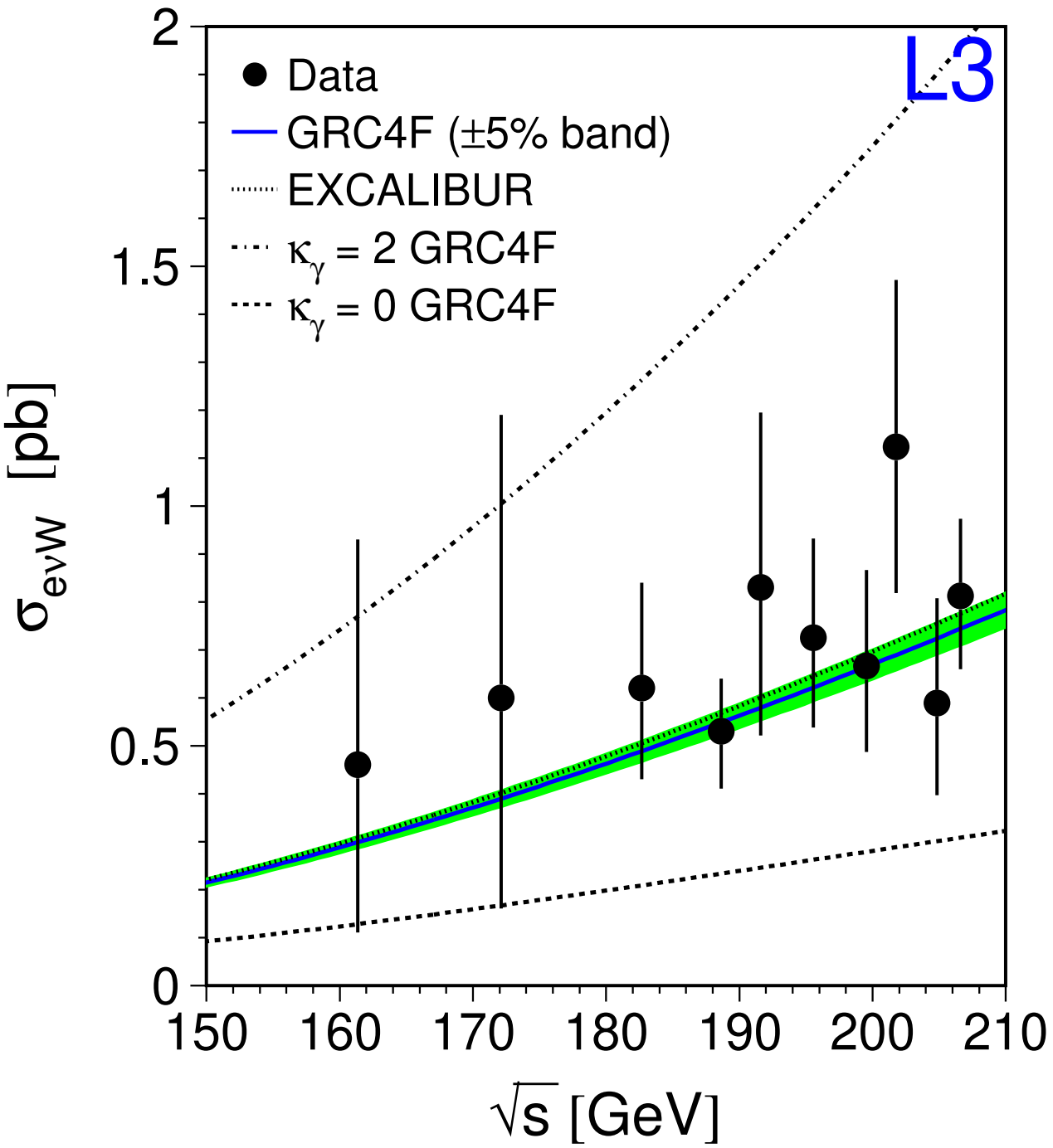

Figure 4: The measured cross section of single W production as a function of $\sqrt{s}$. The solid and dotted lines show predictions of the GRC4F and EXCALIBUR Monte Carlo programs, using the Standard Model value of $\kappa_\gamma = 1$. A $\pm 5\%$ band is added to illustrate the theoretical uncertainty [25]. Possible deviations from the Standard Model for $\kappa_\gamma = 0$ and $\kappa_\gamma = 2$ are illustrated by the dashed and dash-dotted curves.

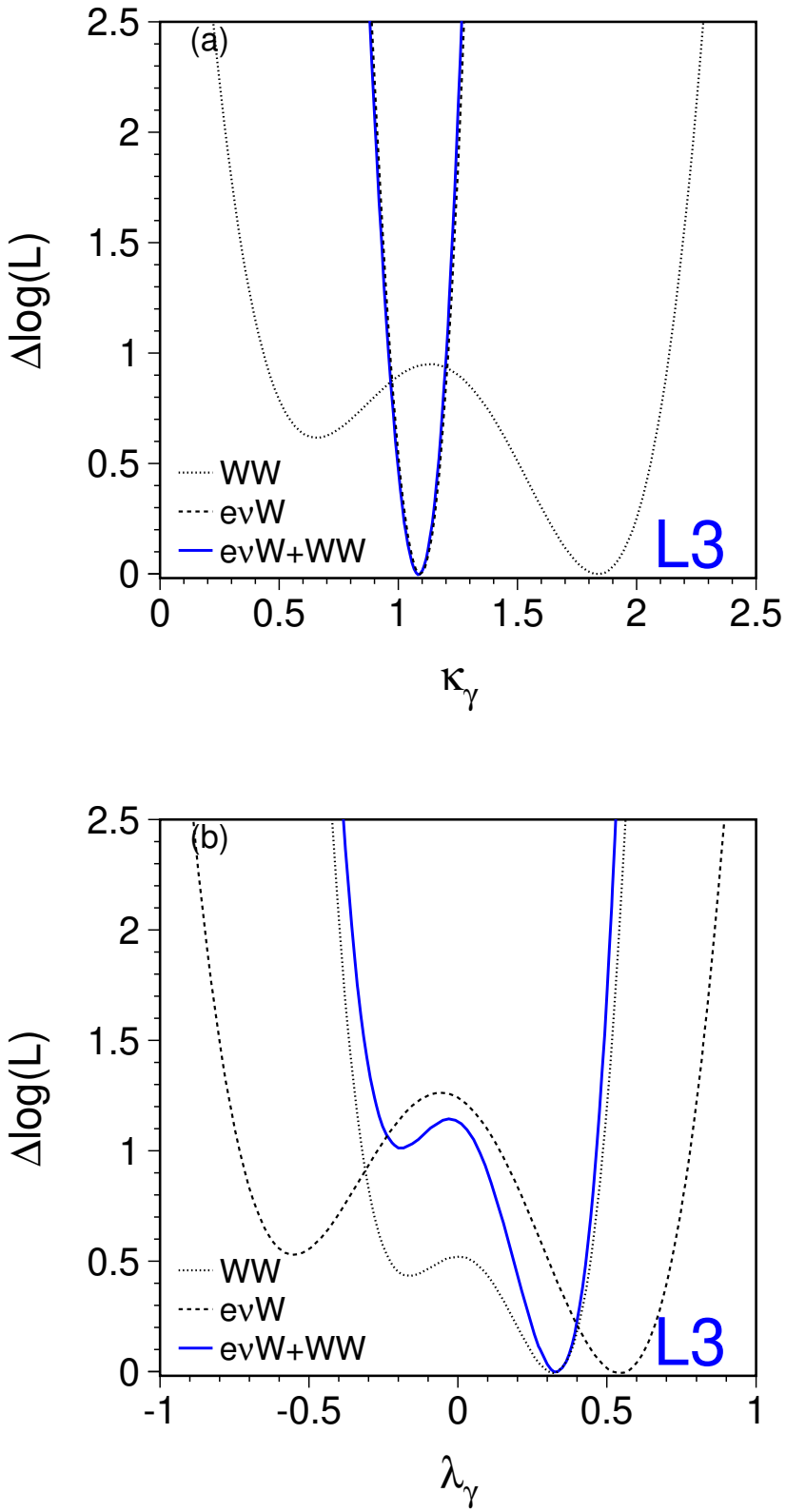

Figure 5: Dependence of the negative log-likelihood function, $\Delta\log(\mathrm{L})$, on the WWγ gauge couplings (a) κ_γ and (b) λ_γ. In each case the other coupling is fixed in the fit to its Standard Model value. For comparison, the likelihood functions are shown for the individual contributions of the signal and the $\mathrm{W^+W^-}$ background. Again, in each case the other process is fixed to its Standard Model expectation.

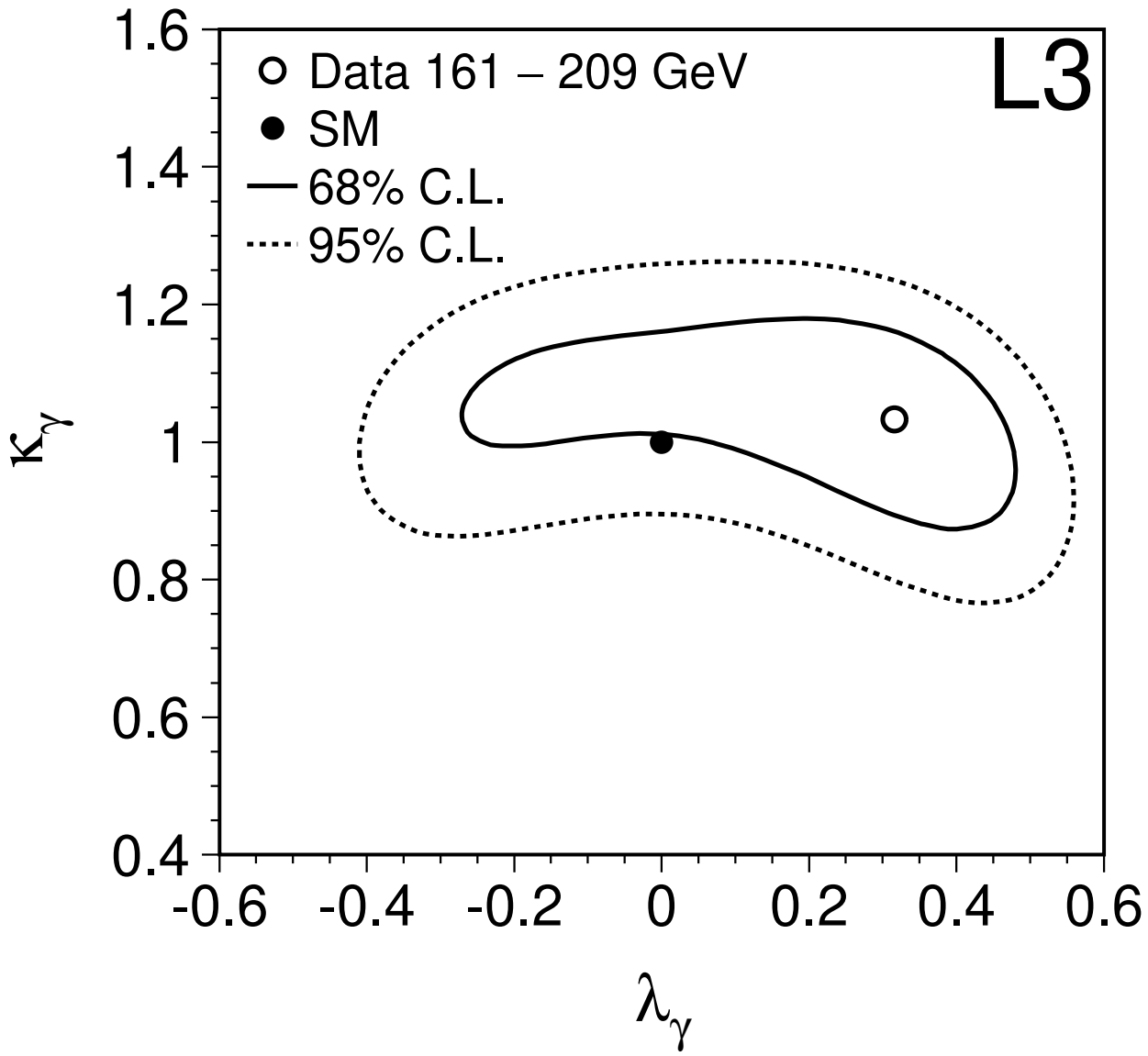

Figure 6: The contours corresponding to 68% and 95% confidence level regions in the $\kappa_\gamma - \lambda_\gamma$ plane. The result of the fit and the Standard Model prediction are also shown.